Eur Biophys J (2010) 39:1537–1545
DOI 10.1007/s00249-010-0611-1

ORIGINAL PAPER

Studies on viral fusion peptides: the distribution of lipophilic and electrostatic potential over the peptide determines the angle of insertion into a membrane

A. Taylor · M. S. P. Sansom

Received: 23 January 2010 / Revised: 6 May 2010 / Accepted: 6 May 2010 / Published online: 25 May 2010

Abstract The oblique insertion of type 1 viral fusion peptides into the cell membrane of the host cell has been shown previously to be an essential element of viral fusion. The actual physical explanation of the cause of the oblique insertion has been the subject of speculation. In this study the physical properties of the fusion peptide surface have been determined computationally and compared to the tilt angles determined both experimentally and by the use of molecular dynamics. It has been shown that the relationship between the distribution of lipophilic potential over the peptide surface and the peptide geometry control the tilt angle of the peptide in a biomimetic DMPC bilayer whereas the depth of penetration into the bilayer appears to be determined by the electrostatic potential and hydrogen bonding at the C-terminus.

Keywords Fusion peptides · Molecular dynamics · Simulations · Biomimetic membranes

Introduction

The fusion between the viral envelope and the cell membrane of the host is a prerequisite of the infection process that results in the transfer of the viral genome into the host cell. The part of the viral envelope protein that mediates the fusion between the viral membrane and that of the host is termed the "viral fusion protein".

While there are similarities between most viral fusion proteins, there are significant differences in structure, which have resulted in their classification into type 1 fusion proteins, as found in viruses such as HIV, influenza, Rubella and Ebola, and type 2 fusion proteins, as found in the yellow fever, dengue, louping ill and tick-borne encephalitis viruses (Kielian and Rey 2006). In the type 1 fusion proteins, there is typically a transmembrane peptide at the C-terminus with which the protein is anchored to the viral envelope, whereas there is a 15–30 residue hydrophobic region at the N-terminus, termed the fusion peptide, which becomes attached to the host cell membrane (Skehel and Wiley 2000).

Our specific interest lies in the structure and function of the fusion peptide segment of the type 1 viral fusion proteins. The structure of these peptide segments and how the structure relates to their function in the bilayer is of great interest. Structural information on the peptide within the cell membrane has been obtained by using NMR (Strandberg et al. 2004) or neutron scattering when the peptide contains deuterium substitution (Bradshaw et al. 2000). Circular dichroism spectroscopy and ATR-FTIR has also give useful information on both the secondary structure and the orientation of the peptide in the membrane (Rodger et al. 2002).

It has been found using the above techniques that the type 1 fusion peptides in the cell membrane or a biomimetic membrane have either an α-helical or partially α-helical structure and that in most cases the peptide is inserted at an angle to the normal to the plane of the bilayer. It has been shown that the fusion peptide segment lowers the phase transition temperature of the bilayer by

Electronic supplementary material The online version of this article (doi:10.1007/s00249-010-0611-1) contains supplementary material, which is available to authorized users.

A. Taylor (✉) · M. S. P. Sansom
Department of Biochemistry, University of Oxford,
South Parks Rd, Oxford OX1 3QU, UK
e-mail: alan.taylor@stx.oxon.org

M. S. P. Sansom
e-mail: mark.sansom@bioch.ox.ac.uk

inducing negative curvature (Tsuboi 1962); this in turn induces hemifusion of the outer leaf of the bilayer with the viral envelope. The fact that most fusion peptides insert into the membrane at an angle of between 25 and 80° to the bilayer normal is consistent with the creation of negative curvature because the angle of insertion will cause a significant increase in the volume of the lipid centre relative to the volume of the headgroup region (Byler and Susi 1986). The forces driving the oblique insertion of the peptide appear to be independent of the membrane charge. Oblique insertion of the Rubella fusion peptide was found in both zwitterionic and negatively charged membranes (Samuel and Shai 2001). The Sendai viral fusion peptide was also found to make an oblique insertion into negatively charged membranes (Rapaport and Shai 1994).

All of the viral tilted peptides have been found to penetrate deeply into the bilayer, the average mass centre being about 1 nm from the centre of the bilayer, however a substantial part of the peptide remains in the headgroup region (Luneberg et al. 1995).

The helical structure of the viral fusion protein is thought to be essential for the fusogenic activity of the type 1 peptides, and it has been stated by Lins that it is only when the helix is amphiphilic, i.e. expressing asymmetric hydrophobicity around the helix, that it develops the oblique insertion of the tilted peptide (Lins et al. 1999). However, it has been argued that the hydrophobic moment of an amphiphilic helix cannot be the sole explanation for the orientation of the peptide (Phoenix and Harris 2003). More recent work has concentrated on the hydrophobicity gradient along the viral fusion peptides; it has been shown by Voneche et al. (1992) that the end to end hydrophobicity plus the amphiphilicity in the SIV and BLV peptides caused the oblique insertion typical of the tilted peptide.

The tilted orientation of the peptide is thought to perturb the regular packing of the lipids and therefore promote membrane destabilisation (Epand and Epand 1994). It has been found that point mutations in the HIV fusion peptide that eliminate the oblique insertion into the membrane also eliminate the fusogenic activity of the peptide (Martin et al. 1996). A molecular dynamics study of the wild type (WT) HIV fusion peptide showed that it inserted into a POPE bilayer at an angle of 45°, but that V2E, G3V, G5V and G10V mutants lie at a much smaller angle to the bilayer surface, and none of these mutants had any fusogenic activity. While these results were obtained using a zwitterionic membrane, in a negatively charged membrane, it was found that mutant V2E made a deeper insertion with a greater tilt angle (Kliger 1997). It may be concluded that the oblique insertion of the viral fusion peptide into the bilayer is essential for fusogenic activity (Kamath and Wong 2002; Wong 2003).

While the oblique insertion of the peptide into the bilayer appears to be a prerequisite for fusogenic activity, the actual mechanism driving the insertion and causing the tilt angle is not so well understood. All the viral fusion peptides are made up primarily of hydrophobic residues. The overall hydrophobicity of the peptide explains the drive for insertion into the bilayer, however other factors appear to determine both the tilt angle and the final location of the peptide in the bilayer.

The effect of individual residues in the Ebola viral fusion peptide on the peptide orientation was studied by modelling mutants and simulating their insertion into a bilayer using the Impala program. The results suggested that the orientation and destabilisation of the bilayer was caused by the end to end difference in hydrophobicity rather than by the properties of any specific residue (Adam et al. 2004).

Although the tilt angles of various fusion peptides have been determined experimentally or by using different molecular dynamics programs, there is no overall study that uses a common program.

In this paper results are presented of molecular dynamics simulations using Gromacs to determine the degree of insertion and angle of orientation of the peptide in a dimyristoyl phosphatidylcholine (DMPC) bilayer and are compared to results obtained experimentally. Their relationship to the distribution of lipophilic and electrostatic potential over the surface of the peptide is explored.

Methods

The peptide models were assembled as α-helices using the Biopolymer (Tripos 2006) program. The peptide molecules were then energy minimised using the Powell (Simplex) method with a gradient of 0.05 kcal mol^{-1} $Å^{-1}$ in the Tripos forcefield; after 1,000 iterations no further significant changes were observed. A surface was then prepared using the Fast Connolly method (Connolly 1983) to give the solvent accessible surface by using a probe radius of 0.14 nm.

The physical properties of the surface were determined using the MOLCAD program (Tripos 2006), and the overall hydrophobicity (lipophilicity potential) of the peptide was determined using the method of Viswanadhan (Ghose et al. 1998). The electrostatic potential of the peptides was measured using the MOLCAD program which calculates the electrostatic potential using the method of Nicholl and Honig (1991). The maximum and minimum electrostatic and lipophilic potentials and the areas of electrostatic and lipophilic maxima and minima were measured. The point of mean lipophilicity of the

peptides was determined using the facility within the MOLCAD program.

The peptides listed in Table 1 were then modelled in a box of dimensions $9.0 \times 6.5 \times 6.0$ nm containing a DMPC bilayer of 128 lipids and 7,360 water molecules, and molecular dynamics was used to simulate their behaviour in a cell membrane mimetic environment. The fusion peptides were inserted into the box normal to the bilayer centered at 6.0 nm with the N-terminus into the headgroup region and the C-terminus in the aqueous region. Alternative starting positions were tried both parallel to the bilayer at the water-headgroup interface and in the aqueous phase but they were not used in later simulations because of the increased length of time required to enter the bilayer. The bilayer simulations were performed using the Gromos 96 forcefield. Energy minimisations were carried out using the steepest descent method for 200 steps of 0.002 ps intervals. A 1 ns equilibration run was carried out with the position of the peptide restrained using harmonic restraints with force constants of 1.0 kJ^{-1} nm^{-2} per atom, applied to all non-hydrogen atoms. Electrostatic energies were calculated using Ewald Particle Mesh with a 1.0 nm cut off for all real space calculations. A 1.0 nm cut off was used for both van der Waal and Coulombic interactions. All simulations were performed at constant temperature, pressure and number of molecules, the temperature of the water, DMPC and peptide being coupled separately.

The Berendsen temperature coupling algorithm (Berendsen et al. 1984) was applied at 310 K with a coupling constant of $\delta_T = 0.1$ ps. The system was semi-isotropically coupled ($x + y$ dimensions were coupled to move as one, the z dimension could move independently of $x + y$) using a Berendsen barostat with a coupling constant $\delta_T = 1$ ps. The system was maintained at 310 K and semi-isotropic pressure using Berendsen coupling. The time steps for integration were 0.002 ps, and co-ordinates and velocities were saved every 5 ps. The LINCS algorithm (Hess et al. 1997) was used throughout to restrain bond lengths.

Table 1 The amino acid sequences of the peptides used in the simulations

Viral fusion peptide	Sequence
HIV	AVGIGALFLGFLGAAG
Rubella	FAGVVLAGAALG
Newcastle	FIGAIIGSVALGVATAAG
Rous	FLGFLLGVGSAIASGVA
Sendai	FFGAVIGTIALGVATSA
Ebola	GAAIGLAWIPYFGPAAE
Flu HA2	GLFGAIAGFIENGWEGMIDG

The whole system was equilibrated by carrying out a molecular dynamics run of 1 ns duration made up of 500,000 steps at 0.002 ps intervals, while keeping the peptide position restrained. A full molecular dynamics run was then carried out with no restraints on the peptide. The MD simulations on the Rous, Rubella and Sendai peptides were continued for 20 ns, however it was observed that convergence occurred between 8 and 10 ns, therefore all other simulations were limited to 10 ns duration. The Sendai and Rubella peptides were subjected to a 300 ns coarse grain MD simulation in DMPC; in both cases the final orientation of the peptide was similar to that obtained after the 10 ns atomistic simulations (Balali-Mood, unpublished results). The simulations were repeated using a "new seed", that is different initial starting parameters; in each case the final orientation of the peptide was the same. The sequences of the viral fusion peptides used are shown in Table 1.

Results

The simulations were analysed using the following Gromacs utilities:

g_rms: Compares two time differentiated conformations of the peptide by computing the root mean square deviation (RMSD) between them. When used to compare the positions of the α-carbons it shows the changes in the conformation of the peptide throughout the simulation.
g_density: Shows the partial densities of the lipid, peptide and water across the box.
g_tiltangle: Computes the tilt angle of the peptide to the bilayer normal by least squares fitting a straight line to the backbone throughout the simulation.
g_hbond: Calculates the hydrogen bonds existing throughout the simulation between the donor and acceptor atoms present based on cut offs for the donor-acceptor distances and angles.

The orientation of the peptides in the DMPC bilayer after the molecular dynamics runs together with the RMSD between the starting and final positions of the alpha carbons are given in Table 2. The tilt angle with reference to the z axis is the mean of the final tilt angles after two 10 ns simulations.

The final tilt angles after 10 ns are compared with those obtained from simulations using alternative force fields and from experimental observations in Table 3.

The results given in Table 3 show that there is a similarity between the tilt angles obtained by molecular dynamics using the Gromacs and CharMM force fields and those obtained experimentally.(Wong 2003; Epand and

Table 2 The orientation and root mean square deviation (RMSD) after 10 ns molecular dynamics

Virus	RMSD Cα	Final tilt angle[a]	Convergence[b]
HIV	0.25	45°	Converged after 6 ns
Rubella	0.58	30°	Converged after 4 ns
Newcastle	0.60	80°	Steady increase converged 8 ns
Rous	0.63	68°	Converged after 6 ns
Sendai	0.44	72°	Converged after 7 ns
Ebola	0.50	75°	Converged after 6 ns
Flu HA2	0.41	62°	Converged after 8 ns

[a] With respect to the *z* axis

[b] Convergence is the point at which no further change in tilt angle occurs

Epand 1994). The tilt angles obtained by atomistic simulations using Gromacs appear to be greater than those obtained using the Monte Carlo method of Impala.

The final position of the peptide in the bilayer and the distribution of headgroups, water, lipid tails and peptide were determined using g_density.

The positions of the peptides in the bilayer after the 10 ns molecular dynamics simulation are given in Table 4.

It can be seen that in most cases the centre of the peptide moves from its starting position centered at 6 nm within the box to a final position after 10 ns further into the bilayer. In the case of HIV, however, the peptide has tilted across the headgroup region while the peptide midpoint has not penetrated further into the bilayer.

The models of two viral fusion peptides prepared using the Biopolymer program showing the distribution of lipophilic potential are given in Figs. 1 and 2. The area of maximum lipophilicity is shown in shades of brown defined by the contour above which the C log P is above 0.010; the area of minimum lipophilicity is shown in blue. The aspects were chosen for each model to give the best view of the distribution of lipophilicity and to demonstrate the significant difference in the morphology of the peptides. The area of maximum electrostatic potential is at the low lipophilic end of the peptide, but the areas of maximum electrostatic potential and minimum lipophilic potential do not necessarily coincide.

Figure 1 shows the distribution of lipophilicity for the Sendai fusion peptide. The four contours of lipophilicity above C log P 0.10 are shown in brown. It may be seen that the Sendai peptide has a fairly straightforward distribution of lipophilicity from the maximum at the N-terminus to the minimum at the C-terminus. This distribution is typical of that of the Sendai, Rous, Rubella and Newcastle peptides. Other peptides have a more complex distribution of lipophilicity as shown by that of HIV in Fig. 2. This distribution is typical of the Ebola, Flu HA2 and HIV peptides, which have a lipophilicity midpoint much nearer to the C-terminus. The details of the extent and distribution of lipophilicity and electrostatic potential are given in Table 5.

It can be seen that there is a large difference in the distribution of lipophilicity with the different peptides. The actual scale of lipophilicity is the same for all peptides but

Table 3 A comparison of tilt angles with respect to the *z* axis obtained by different methods

Virus	Impala (Lins et al. 2001)	CharMM (Wong 2003)	Experimental (Epand and Epand 1994)	Gromacs (2009)	
				Average tilt angle	Final tilt angle
HIV/SIV	45°	40–45°	55° (SIV)	49°	45°
Rubella	13°	–	–	61°	60°
Newcastle	17°	–	–	60°	80°
Rous	27°	–	–	58°	68°
Sendai	18°	–	–	52°	63°
Flu HA2	–	–	45–66°	58°	62°

Table 4 Orientation and position of the peptide after 10 ns molecular dynamics simulation

Virus	Peptide position (nm)	Peptide midpoint (nm)	Distribution in bilayer[a]
HIV	4.5–7.2	6.3	Across HG region
Rubella	4.4–7.0	5.6	Across HG region
Newcastle	3.6–6.0	4.7	Across tails
Rous	3.8–7.0	5.4	Across tails and HG region
Sendai	3.6–7.5	4.5	Across tails and HG region
Ebola	3.6–6.7	4.5	Across tails and a part of HG
Flu HA2	3.8–7.0	4.9	Across HG region + some tails

HG Headgroup

[a] Position of the peptide within the bilayer

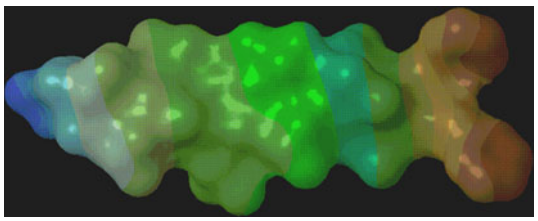

Fig. 1 Connolly surface of the Sendai fusion peptide (area of maximum lipophilic potential shown in *brown* and the area of minimum lipophilicity in *blue*)

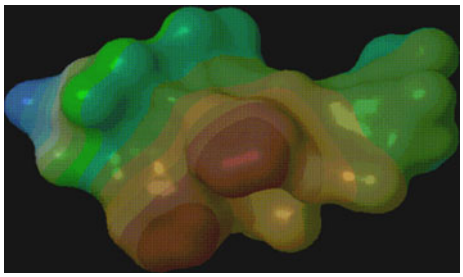

Fig. 2 Connolly surface of the HIV fusion peptide (area of maximum lipophilic potential shown in *brown* and the area of minimum lipophilicity in *blue*)

the difference in area of maximum lipophilicity ranges from 0.88 nm^2 for Newcastle to 2.50 nm^2 for Flu HA2. The area of maximum electrostatic potential at or close to the C-terminus does not differ much among the peptides, only Ebola and Flu HA2 with aspartate and glutamate residues at the C-termini are significantly different.

The relationships between the lipophilic potential, area of maximum lipophilicity, electrostatic potential and area of maximum electrostatic potential to the tilt angle were explored. It was thought that the tilt angle may be the result of a turning moment about the midpoint of the molecule. An attempt was made to get over the problem of the varying distribution of lipophilicity by considering only the area above the top four contours of maximum lipophilic potential and treating this area as proportional to the lipophilic turning force. The product of the area of maximum lipophilicity and distance from the lipophilic midpoint to the C-terminus was found to give an excellent correlation (R^2 0.97) with the tilt angle determined for the peptides studied as shown in Fig. 3.

The correlation between the electrostatic properties and tilt angle was also investigated, however no correlation between the tilt angle and the maximum electrostatic potential or the area of maximum electrostatic potential could be found nor was any found between the ratio of the lipophilic properties of the N-terminus and the electrostatic properties at the C-terminus.

The distribution of the peptide-water and the peptide-DMPC hydrogen bonds was determined throughout the simulation using Gromacs g_bond (Supplementary Table 1). It was found that as the peptide entered the bilayer the number of peptide-water H bonds at the C-terminus changed very little and when they were lost they were replaced by peptide-DMPC hydrogen bonds. However, for the remainder of the peptide there is a significant loss of peptide-water H bonds which are replaced by peptide-DMPC hydrogen bonds as the peptide moves into the bilayer. At the N-terminus where it enters the anhydrous hydrocarbon region of the bilayer there is a permanent loss of peptide hydrogen bonds. The number of lost hydrogen bonds is indicative of the depth of penetration into the lipid tails region of the bilayer with Ebola, Newcastle and Flu HA2 giving the most penetration as may be seen in Supplementary Fig. 1.

In order to explore the effect of changes in the extent and distribution of lipophilicity on the behaviour of the peptide in a bilayer, a number of point mutations were made in each peptide. The distribution of lipophilic and electrostatic potential was determined using the same methods used for the WT peptides and related to their behaviour in the bilayer. The mutant peptides used in the study are listed in Table 6.

Simulations with the mutant peptides were run for 10 ns using the same conditions as before. The results of the simulations are shown in Table 7. It can be seen that in most cases there is greater variability in the orientation of the mutant peptides compared to the corresponding wild type. Also it is evident that a single point mutation can make a big difference in the tilt angle of the peptide in the bilayer.

Table 5 The relationship of tilt angles of viral fusion peptides to surface physical properties

VFP	Tilt angle[a]	ES area max (nm^2)	Lip area max (nm^2)	Distance from lipophilic midpoint to C-terminus (nm)	Lip (nm^2) × distance (nm)
HIV	45	0.51	1.24	0.85	1.054
Rubella	30	0.54	0.98	0.7	0.686
Newcastle	80	0.53	0.88	2.0	1.766
Rous	68	0.55	1.24	1.2	1.488
Sendai	63	0.50	1.61	1.0	1.610
Ebola	75	0.66	1.26	1.2	1.512
Flu HA2	62	0.68	2.50	0.55	1.375

VFP Viral fusion peptides, *ES area max* area of maximum electrostatic potential, *Lip area max* area of maximum lipophilicity

[a] With respect to *z* axis

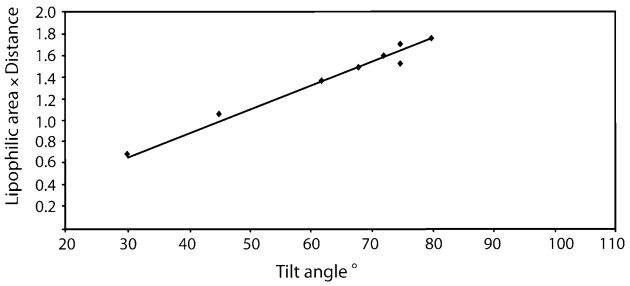

Fig. 3 Correlation between tilt angle and the product of maximum lipophilic area and distance from lipophilic midpoint to C-terminus

Table 6 The point mutations of the viral fusion peptides. The HIV mutants are those used by Wong (2003)

Mutant	Sequence
HIV M1	G10V
HIV M2	A1FV2FF8AF11V
HIV M3	G3V
HIV M4	G5V
Rubella M1	F1G
Rubella M2	G12E
Rous M1	F1G
Rous M2	F1GF4G
Rous M3	A17V
Sendai M1	F1S
Sendai M2	F1SF2G

The area of maximum lipophilicity and the distance from the lipophilic midpoint to the C-terminus were determined as before; the results are given in Table 8.

It can be seen that there is a large difference in the distribution of lipophilicity with the different peptides. The area of maximum lipophilicity ranges from 0.51 nm^2 for Rous M1 to 4.79 nm^2 for Rous M2. The area of maximum electrostatic potential at or close to the C-terminus does not differ much among the peptides.

It is not easy to correlate the changes in maximum lipophilicity at the N-terminus with the point mutations. However, it is apparent that if increasing the overall lipophilicity pushes the lipophilic midpoint nearer to the C-terminus then the tilt angle is not increased. This is particularly noticeable with the Rubella M1 and Rous M2 mutants, where there is a significant increase in area of maximum lipophilicity, but as the midpoint is now much closer to the C-terminus, the tilt angle is not increased in proportion. The HIV mutants G3V, G5V and G10V all increase the lipophilic area but as the midpoint becomes nearer to the C-terminus, the tilt angle is not increased significantly. The increase causes the peptide to penetrate deeper into the bilayer by between 1 and 1.6 nm (Fig. 4).

The principal limitation of this study is the simplicity of the model used compared to the complexity of the distribution of lipophilicity over the surface of the peptide. The problem can best be seen by comparing the results from the four WT peptides with a simple distribution of lipophilicity which had a correlation coefficient R^2 of 0.99 compared to the plot for all the WT peptides (Fig. 3) which gave a R^2 of 0.97. The correlation coefficient for the mutant peptides was lower with R^2 of 0.86 due to the difficulty of determining a stable "final" tilt angle after 10 ns and the more complex distribution of lipophilicity.

Discussion

Much thought has been given to the hydrophobic and amphipathic nature of the viral fusion peptides and the effect on their behaviour in the cell membrane. It is the hydrophobic nature of the peptide that causes it to be driven from the aqueous phase into the lipid bilayer; however once it is in the headgroup region, the hydrophobic force declines rapidly as the peptide approaches the anhydrous hydrocarbon region of the bilayer. Therefore the

Table 7 Orientation and root mean square deviation (RMSD) of the peptides after 10 ns molecular dynamics simulation

Virus	RMSD Cα	Final tilt angle[a]	Comments
HIV M1	0.50	54	Fluctuates around 30° 2–8 ns
HIV M2	0.40	70	Large fluctuation 20–60°, stable after 8 ns
HIV M3	0.15	45	Large fluctuation 20–60°
HIV M4	0.42	62	Steady increase to 8 ns
Rubella M1	0.60	55	Large fluctuation 20–90° over 1–9 ns
Rubella M2	0.55	35	Large fluctuation 5–60°
Rous M1	0.50	20	Large fluctuation 5–60°
Rous M2	0.38	35	Large fluctuation 10–50°
Rous M3	0.58	63	Small fluctuation
Sendai M1	0.60	60	Large fluctuation 10–75°
Sendai M2	0.60	50	Stable after 5 ns

[a] With respect to the z axis

Table 8 Analysis of VFP mutants in DMPC bilayers

Mutant VFP	Tilt angle[a]	ES area max (nm^2)	Lip area max (nm^2)	Distance from lipophilic midpoint to C-terminus (nm)	Lip (nm^2) × distance (nm)
HIV M1	54	0.51	1.63	0.65	1.060
HIV M2	70	0.47	1.31	1.0	1.310
HIV M3	45	0.51	1.63	0.55	0.897
HIV M4	62	0.51	1.73	0.65	1.125
Rubella M1	55	0.60	4.70	0.24	1.128
Rubella M2	35	0.52	0.60	0.9	0.540
Rous M1	20	0.55	0.51	0.5	0.255
Rous M2	40	0.54	4.79	0.2	0.958
Rous M3	63	0.54	1.03	1.05	1.082
Sendai M1	60	0.51	0.72	1.35	0.972
Sendai M2	50	0.52	1.65	0.6	0.990

VFP Viral fusion peptides, *DMPC* dimyristoyl phosphatidylcholine, *ES area max* area of maximum electrostatic potential, *Lip area max* area of maximum lipophilicity

[a] With respect to z axis

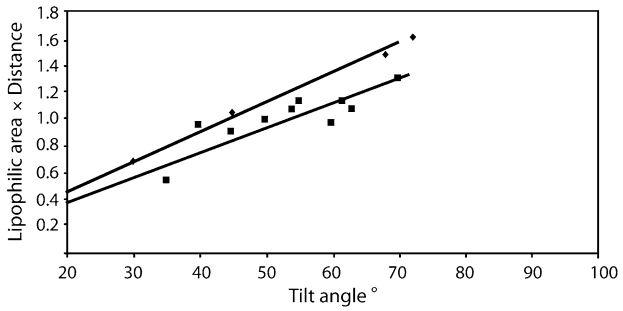

Fig. 4 Correlation between tilt angle and the product of lipophilicity and distance from lipophilic midpoint to C-terminus (*squares* mutant peptides, *diamonds* WT peptides)

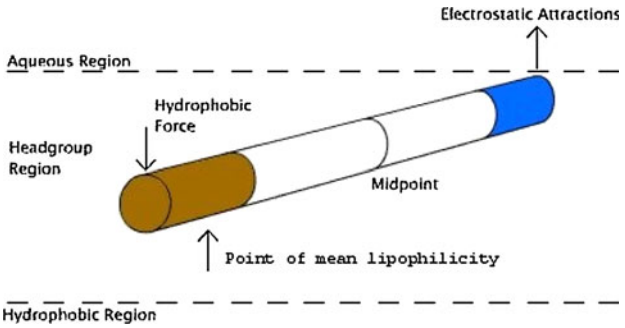

Fig. 5 Distribution of turning forces on a tilted peptide

distribution of lipophilicity becomes of less importance as the peptide passes deeper into the headgroup region.

It would appear that the C-terminus is in effect an anchor caused by the hydrogen bonding to the aqueous headgroup region. The lipophilicity of the peptide in the region approximating to the N-terminus causes the N-terminus to be pushed deeper into the bilayer; however the actual tilt angle appears to be determined by the length of the peptide and the distribution of lipophilicity over the surface of the peptide. While it might appear that lipophilicity at the extreme of the N-terminus would cause a deeper insertion into the bilayer and therefore a greater tilt angle, it should be recognised that the hydrophobic force decreases rapidly as the peptide approaches the anhydrous tail region. It is thought that this is why the lipophilic midpoint is important; significant lipophilicity near the geometric midpoint of the peptide will cause the N-terminus to be more deeply inserted (Fig. 5).

The polar headgroup region has to be the site of fusion peptide adsorption onto the bilayer. This region changes from the hydrocarbon phase of the lipid tails, dielectric $\varepsilon = 2$, to the aqueous phase with a dielectric of $\varepsilon = 80$. In reality the headgroup region has a dielectric constant in the range $\varepsilon = 25$–40 (Ashcroft et al. 1981). However, there is no doubt that the correct model is that described by White et al. (2001) in which the probability distribution of water molecules and lipid headgroups declines gradually with a concomitant fall in dielectric constant towards the hydrocarbon core of the bilayer (Simonsen and Perahia 1995).

While Efremov et al. (1999) found no evidence for interactions between the polar headgroups and the chemical groups on the backbone and side chains of the peptide, both Han et al. (1999) and Bechor and Ben-Tal (2001) argue for their importance. Bechor concludes that there is a desolvation free energy difference of 8–14 kcal mol^{-1} between a peptide lying horizontal at the headgroup-water interface and the oblique insertion, and they state that how this difference is overcome remains unexplained.

The molecular dynamics simulations of the fusion peptides in the DMPC bilayers confirm the above conclusions. In all cases there is a significant exchange of peptide-water hydrogen bonds to peptide-DMPC hydrogen bonds in the course of the simulation, with the peptides coming to reside across the headgroup region of the bilayer at approximately the same angles as reported in the literature.

The changes predicted by Gromacs (2009) in the number of hydrogen bonds between the headgroups and water due to the insertion of the peptide have been confirmed experimentally (Buzon et al. 2005). Infrared spectroscopy was used to study the effect of peptide binding on the hydration state of the phospholipid ester carbonyl groups. The lipid carbonyl absorbance region lies between 1,700 and 1,750 cm^{-1}; a band at 1,742 cm^{-1} corresponds to the carbonyls that are not hydrogen bonded to water, while a band at 1,727 cm^{-1} corresponds to the carbonyls that are hydrogen bonded to water. When the peptide is inserted into the bilayer the band at 1,742 cm^{-1} attributed to the dehydrated carbonyls increases, while the band at 1,727 cm^{-1} decreases. The hydrogen bonding interaction of the peptide with the headgroups is confirmed at the expense of the headgroup water hydrogen bonds, the insertion of the peptide therefore having a dehydrating effect at the lipid water interface.

If one considers the headgroup probability distribution described, it is obvious that the dielectric constant will decline along the same curve as the probability of water and headgroups. Therefore a hydrophobic peptide with a varying distribution of lipophilic potential over the surface will be driven by a declining hydrophobic force into the bilayer, while parts of the peptide are retained by the headgroup region because of the electrostatic attractions. It is reasonable to speculate that because there is a nonlinear decline in polarity and hydrophobicity from the outer headgroup region to the hydrocarbon core, a peptide with differences in lipophilic and electrostatic potential reaches an equilibrium within the headgroup region, depending on the size of the difference of the lipophilic and electrostatic regions of the peptide. It is thought that the same principles will apply to fusion peptides with different structures. In the case of HIV the fusion peptide adopts a beta sheet conformation when attached to the N-heptad repeat of gp41 (Sackett et al. 2006). This mechanism has also been found to apply with the type 2 viral fusion peptides of Semliki Forest virus and hepatitis C virus, even though the overall conformation of the fusion peptide is in the form of a loop within the viral envelope protein and is quite different from the type 1 fusion peptides. MD simulations of these peptides in a DMPC bilayer using Gromacs gave tilt angles similar to those reported in this paper (Taylor et al. 2009).

The results from the simulations with the type 1 mutant peptides show that even a single point mutation can make a big difference to the tilt angle within the bilayer.

The variability of the tilt angle throughout the simulations and apparent instability of the orientation in the bilayer caused by point mutations of the peptide were unexpected. It would appear that even a single point mutation creates a peptide that is far less likely to find a stable low energy position in the bilayer. It could be that evolution has found the sequence that gives the optimum stable tilt angle to cause membrane fusion, and deviations from this sequence produce a peptide that cannot find a stable orientation in the bilayer.

Acknowledgments The determination of the physical properties of the peptides was carried out using the Sybyl molecular modelling facility at the University of Central Lancashire.

References

Adam B, Lins L, Stroobant V, Thomas A, Brasseur R (2004) Distribution of hydrophobic residues is crucial for the fusogenic properties of the Ebola virus GP2 fusion peptide. J Virol 78:2131–2136

Ashcroft RG, Carter HG, Smith JR (1981) The molecular organisation of bimolecular lipid membranes: the dielectric structure of the hydrophilic/hydrophobic interface. Biochem Biophys Acta 643:191–204

Bechor D, Ben-Tal N (2001) Implicit solvent model studies of the interactions of the influenza hemagglutinin fusion peptide with lipid bilayers. Biophys J 80:643–655

Berendsen HJC, Postma JPM, van Gunsteren NF, Dinola A, Haak JR (1984) Molecular dynamics with coupling to an external bath. J Chem Phys 81:3684–3690

Bradshaw JP, Darkes MJ, Harroun TA, Epand RM (2000) Oblique membrane insertion of viral fusion peptides probed by neutron diffraction. Biochemistry 39:6581–6585

Buzon V, Padros E, Cladera J (2005) Interaction of fusion peptides from HIV gp41 with membranes: a time resolved membrane binding, lipid mixing and structural study. Biochemistry 44:13354–13364

Byler D, Susi H (1986) Examination of the secondary structure of proteins by deconvolved spectra. Biopolymers 25:469–487

Connolly ML (1983) Solvent—accessible surfaces of proteins and nucleic acids. Science 221:709–713

Efremov RG, Nolde DE, Volynsky PE, Chernyasky AA, Dubovskii PV, Arseniev AA (1999) Factors important for fusogenic activity of peptides: molecular modelling study of analogs of fusion peptide of influenza virus hemagglutinin. FEBS Lett 462:205–210

Epand RM, Epand RF (1994) The relationship between the infectivity of influenza virus and the ability of its fusion peptide to perturb bilayers. Biochem Biophys Res Comm 202:1420–1425

Ghose AK, Viswanadhan VN, Wendaloski JJ (1998) Prediction of lipophilic properties of organic molecules using fragmental methods: an analysis of A LogP and C LogP methods. J Phys Chem A 102:3762–3772

Gromacs (2009) http://www.gromacs.org

Han X, Steinauer SA, Tamm LK (1999) Interaction of mutant influenza hemagglutinin fusion peptides with lipid bilayers: probing the role of hydrophobic residue size in the region of the fusion peptide. Biochemistry 38:15052–15059

Hess B, Bekker H, Berendsen HJC, Fraaije JG (1997) LINCS: a linear constraint solver for molecular simulations. J Comp Chem 18:1463–1472

Kamath S, Wong TC (2002) Membrane structure of the HIV gp41 fusion domain by molecular dynamics simulations. Biophys J 83:135–143

Kielian M, Rey FA (2006) Virus membrane-fusion proteins: more then one way to make a hairpin. Nat Rev Microbiol 1:67–76

Kliger Y (1997) Fusion peptides derived from the HIV type 1 glycoprotein 41 associate within phospholipid membranes and inhibit cell-cell fusion. A structure-function study. J Biol Chem 272:13496–13505

Lins L, Thomas SA, Piullot T, Rosseneau M, Brasseur R (1999) Molecular determinants of the interaction between the C-terminal domain of β-amyloid peptide and apolipoprotein α-helices. J Neurochem 73:758–769

Lins L, Charloteaux B, Thomas A, Brasseur R (2001) Computational study of lipid destabilising protein fragments: towards a comprehensive view of tilted peptides. Proteins 44:435–437

Luneberg J, Martin I, Nussler F, Ruyschaert JM, Herrman A (1995) Structure and topology of the influenza viral fusion peptide in a lipid bilayer. J Biol Chem 270:1139–1148

Martin I, Schaal A, Scheid A, Ruyschaert JM (1996) Lipid membrane fusion induced by HIV type1 gp41 N-terminal extremity is determined by its orientation in the lipid bilayer. J Virol 70:298–304

Nicholl A, Honig B (1991) A rapid finite differential algorithm utilising over relaxation to solve the Poisson-Boltzmann equation. J Comp Chem 12:435–445

Phoenix D, Harris F (2003) Is the use of hydrophobic moment a sound basis for predicting the structure and function relationships of membrane interactive helices. Curr Prot Pept Sci 4:357–366

Rapaport D, Shai Y (1994) Interaction of fluorescently labelled analogues of the amino terminal fusion peptide of Sendai virus with phospholipid membranes. J Biol Chem 269:15124–15131

Rodger A, Norden B, Halsall DJ, Woolhead CA, Robinson C, Seymour M (2002) Flow oriented linear dichroism to probe protein orientation in membrane environments. Phys Chem Chem Phys 4:4051–4057

Sackett K, Wexler-Cohen Y, Shai Y (2006) Characterisation of the HIV N terminal fusion peptide containing region in context of key gp41 fusion conformation. J Biol Chem 281:21755–21762

Samuel O, Shai Y (2001) Participation of two fusion peptides in measles virus induced membrane fusion: emerging similarity with other paramyxoviruses. Biochemistry 40:1340–1349

Simonsen T, Perahia D (1995) Internal and interfacial properties of cytochrome c from molecular dynamics in aqueous solution. PNAS 92:1082–1086

Skehel JJ, Wiley DC (2000) Receptor binding and membrane fusion in virus entry of the influenza haemagglutinin. Annu Rev Biochem 61:531–569

Strandberg JP, Ozdirekean S, Rijkers DTS, Koeppe RE, Liskamp RMJ (2004) Tilt angles of transmembrane model peptides in oriented and non-oriented bilayers as determined by ^{2}H solid state NMR. Biophys J 86:3709–3721

Taylor A, O'Leary JM, Pollock S, Zitzmann N (2009) Conservation of hydrophobicity within viral envelope glycoproteins reveals a putative hepatitis C virus fusion peptide. Protein Pept Lett 16:815–822

Tripos (2006) http://www.tripos.com

Tsuboi M (1962) Infrared dichroism and molecular conformation of α-form poly-g-benzyl-l-glutamate. J Polym Sci 59:139–153

Voneche JJ, Portetelle D, Kettman R, Willems L, Ruyschaert JM, Brasseur R (1992) Fusogenic segments of BLV and SIV are interchangeable and mediate fusion by means of oblique insertion in the lipid bilayer of their target cells. PNAS 89(9):3810–3814

White SH, Ladokhin AS, Jayasinghe S, Histova K (2001) How membranes shape protein structure. J Biol Chem 276:32395–32398

Wong TC (2003) Membrane structure of the HIV gp41 fusion peptide by molecular dynamics simulations of the glycine mutants. Biochim Biophys Acta 1609:45–54